However, at 0° in the laboratory we have also measured directly the deuteron flux[15] and find in agreement with Overseth *et al.*[16]

$$\frac{d\sigma}{d\Omega}(d,180°)=(11\pm2)\ \mu\text{b/sr}. \tag{9}$$

We therefore conclude that the contribution of the (np) final-state interaction (which will be mainly due to the $^1S_0$ state) is of the order

$$\frac{d\sigma}{d\Omega}(0°,\text{ final state})=(2\pm3)\ \mu\text{b/sr}. \tag{10}$$

[15] We did measure the slow deuterons, e.g., those produced at 180° in the c.m., which correspond exactly to the π mesons observed in process 5.

[16] O. Overseth, R. Heinz, L. Jones, M. Longo, D. Pellett, M. Perl, and F. Martin, Phys. Rev. Letters **13**, 59 (1964).

ACKNOWLEDGMENTS

We are indebred for the advice and assistance of our colleagues Dr. S. J. Lindenbaum, Dr. S. Ozaki, and Dr. E. J. Sacharidis who participated in the K-meson production experiment. We also acknowledge the efficient cooperation of the Cosmotron operating and supporting staffs that made this experiment possible.

PHYSICAL REVIEW VOLUME 142, NUMBER 4 FEBRUARY 1966

Proton Form Factors from Elastic Electron-Proton Scattering*

T. JANSSENS,† R. HOFSTADTER, E. B. HUGHES,‡ AND M. R. YEARIAN
Department of Physics and High-Energy Physics Laboratory, Stanford University, Stanford, California
(Received 4 October 1965)

Absolute measurements of the elastic electron-proton cross section have been made with a precision of about 4% for values of the square of the four-momentum transfer, q^2, in the range 6.0 to 30.0 F^{-2} and for electron scattering angles in the range 45° to 145°. To within the experimental errors, it is found that the charge and magnetic form factors of the proton have a common dependence on q^2 when normalized to unity at $q^2=0$, and that an accurate representation of the behavior of the form factor and that of the cross sections themselves can be given in terms of a three-pole approximation to the dispersion theory of nucleon form factors.

I. INTRODUCTION

THE elastic scattering of electrons by protons is described to lowest order in quantum electrodynamics by means of the Rosenbluth equation.[1] In this approximation a single virtual proton is exchanged between the electron and proton and the structure of the proton is represented by two electromagnetic form factors which are functions of q^2, the square of four-momentum carried by the virtual photon.[2]

Earlier measurements of the elastic electron-proton cross section have been carried out at Stanford,[3,4] and more recently at other laboratories,[5–12] for values of q^2 up to 125.0 F^{-2}. In the present experiment we have made extensive measurements of this cross section for values of q^2 in the range 4.0 to 30.0 F^{-2} and for values of the electron scattering angle in the range 45.0 to 145.0°. The statistical accuracy of the data is about 2% and a determined effort has been made to minimize systematic errors.

Precise measurements of the elastic electron-proton cross section are of interest both because of their fundamental significance and also because they provide standard experimental quantities against which the results of other electron-scattering measurements are frequently normalized. The results of the present experiment are used to test the validity of the Rosenbluth equation and to determine the electromagnetic form factors of the proton. The form factors are im-

* This work was supported in part by the U. S. Office of Naval Research Contract [Nonr 225(67)] and the U. S. Air Force Office of Scientific Research.

† Present address: Aerospace Corporation, El Segundo, California.

‡ Present address: Princeton University, Princeton, New Jersey.

[1] M. N. Rosenbluth, Phys. Rev. **79**, 615 (1950).

[2] D. R. Yennie, M. Lévy, and D. G. Ravenhall, Rev. Mod. Phys. **29**, 144 (1957).

[3] E. E. Chambers and R. Hofstadter, Phys. Rev. **103**, 1454 (1956).

[4] F. Bumiller, M. Croissiaux, E. Dally, and R. Hofstadter, Phys. Rev. **126**, 1623 (1961).

[5] P. Lehman, R. Taylor, and R. Wilson, Phys. Rev. **126**, 1183 (1962).

[6] D. J. Drickey and L. N. Hand, Phys. Rev. Letters **9**, 521 (1962).

[7] D. Yount and G. Pine, Phys. Rev. **128**, 1942 (1962).

[8] P. A. M. Gram and E. B. Dally, Bull. Am. Phys. Soc. **1**, 489 (1962).

[9] D. N. Olson, H. F. Schopper, and R. R. Wilson, Phys. Rev. Letters **6**, 286 (1961).

[10] K. Berkelman, M. Feldman, R. M. Littauer, G. Rouse, and R. R. Wilson, Phys. Rev. **130**, 2061 (1963).

[11] B. Dudelzak, G. Sauvage, and P. Lehman, Nuovo Cimento **28**, 18 (1963).

[12] K. W. Chen, A. A. Cone, J. R. Dunning, Jr., S. F. G. Frank, N. F. Ramsey, J. K. Walker, and R. Wilson, Phys. Rev. Letters **11**, 561 (1963).

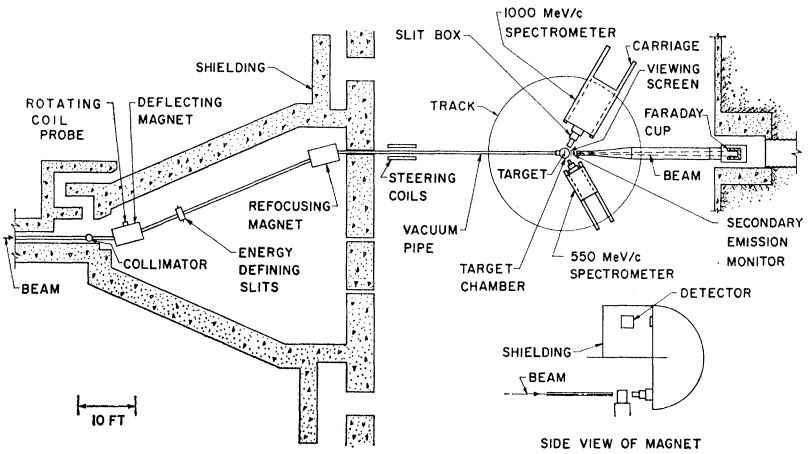

FIG. 1. A schematic diagram of the beam-transport system and the experimental area.

portant phenomenological properties of the proton and are used to interpret the results of many other experiments involving the electromagnetic interactions of the proton. The form factors are also the fundamental data against which theoretical descriptions of nucleon form factors are tested. One such description is discussed in a later section of this paper.

In Sec. II we describe the refinements of the experimental technique used in the present experiment. In Sec. III we give the experimental cross sections and the values of the form factors derived from them. A representation of these form factors in terms of a three-pole approximation to the dispersion theory of nucleon form factors is given in Sec. IV and the conclusions of the present work are summarized in Sec. V.

II. EXPERIMENTAL METHOD

The experimental arrangement is shown in Fig. 1. The electron beam from the Stanford Mark III linear accelerator, with an incremental energy width of 0.5%, was scattered from a thin liquid-hydrogen target. After passing through the target the intensity of the electron beam was monitored by means of a Faraday cup. The scattered electrons were accepted, focussed and analyzed in momentum by a 72 in. double-focusing magnetic spectrometer and detected by a counter located in the focal plane of the spectrometer.

The experimental method is very similar to that previously used by Bumiller *et al.*[4] The most important differences between the present experiment and the previous work are associated with (a) the use of an electron counter with a wide momentum acceptance, (b) the use of a thin liquid-hydrogen target, and (c) a precise floating-wire recalibration of the magnetic-deflection system which defines the energy of the electrons emerging from the accelerator. These and other improvements will be discussed in this section.

The electron-proton cross section is given by the following equation:

$$d\sigma(E_0,\theta)/d\Omega = C\alpha\beta/N_0N_T\Delta\Omega, \quad (1)$$

where C is the number of scattered electrons detected by the counter, E_0 is the incident-electron energy, θ is the scattering angle, N_0 is the number of incident electrons, N_T is the number of target nuclei/cm^2, $\Delta\Omega$ is the solid angle defined by the spectrometer entrance slits, α is counting-rate correction factor, β is the radiative correction factor.

The methods by which the above quantities were determined together with the errors involved in their determination are described in the following paragraphs.

(a) The Electron Counter

A large Lucite Čerenkov counter was designed for use in the present experiment. A shaped Lucite block was viewed from the rear by two RCA 7046 photomultipliers and the outputs were added in order to optimize the over-all pulse-height distribution. The counter had an aperture of 26.54 cm, which corresponded to a momentum acceptance of 3.5%, and was capable of measuring an elastic electron-proton cross section with a single momentum setting of the spectrometer. A study of the pulse-height distribution indicated that under typical operating conditions the efficiency of the counter for detecting electrons was about $(99.5\pm0.5)\%$.

For convenience in identifying the elastic-scattering peak and to be sure that this peak was totally accepted by the Čerenkov counter, a ladder counter consisting of ten small plastic scintillation counters was placed immediately in front of the Čerenkov counter and operated in coincidence with it. The primary data of the experiment, however, came from the Čerenkov counter alone.

(b) The Incident-Electron Energy

An accurate knowledge of the incident-beam energy is essential since, for example, an error of 0.5% in the electron energy can produce an error of as much as 2.0% in the measured cross section at certain angles. The necessary calibration of the magnetic deflection

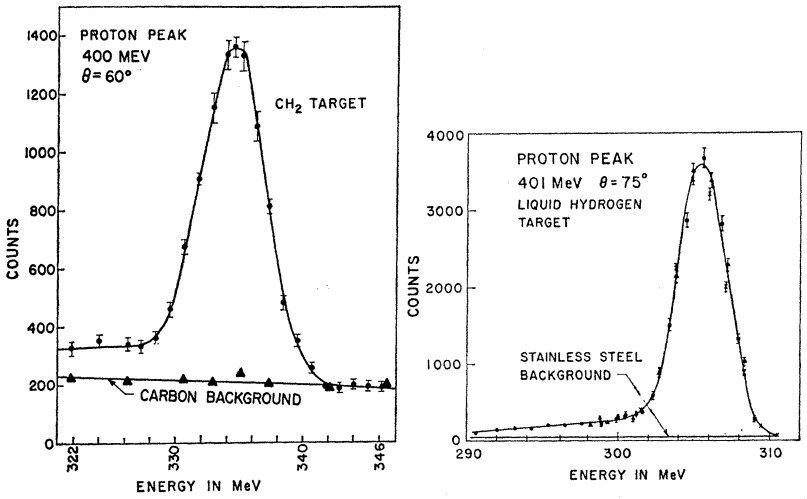

FIG. 2. This figure illustrates the relative sizes of the background subtractions required when an elastic electron-proton cross section is measured using a solid polyethylene target and a liquid-hydrogen target. The data shown in the right-hand side of this figure were obtained using an electron counter of small momentum acceptance and not the counter designed for use in the present experiment.

system at the end of the accelerator was accomplished by means of the floating-wire technique. A wire was suspended using a special air-bearing pulley[13] and its position measured at three points along the beam trajectory. By this method the momentum corresponding to a particular trajectory through the system was determined to about 0.1% and the central momentum of an actual electron beam to about 0.2%. During the calibration the signals from a nuclear magnetic resonance probe and from a rotating-coil fluxmeter in a deflecting magnet were calibrated absolutely in terms of the momentum accepted by the deflection system so that any subsequent electron energy could be obtained with the above precision.

(c) The Target

The liquid-hydrogen target was nominally 0.953 cm thick in the beam direction and the target walls were made of 0.0254 mm stainless steel foils. The design of these targets is described by Chambers *et al.*[14]

The advantage of the target used in the present experiment over the polyethylene target previously used by Bumiller *et al.*, is mainly associated with the much smaller background subtraction required. This difference is illustrated in Fig. 2 in which the left-hand figure shows an elastic hydrogen peak measured at 400 MeV and 60° using a polyethylene target and the right-hand figure shows a similar peak measured using a thin liquid-hydrogen target. As can be seen, the background scattering observed from the walls of the liquid target is much less than the scattering observed from the carbon in the solid target.

The liquid hydrogen in the target was normally maintained in equilibrium with a gas pressure of 25 psi. Under these conditions the walls of the target tended to bulge outward in the vacuum space and it became necessary to measure the actual thickness of the target in the beam direction. This was done by focusing a traveling microscope on the outer walls of the target from a direction perpendicular to the beam direction. In this way the total thickness of the target was found to be (1.092±0.004) cm. The reliability of this method was checked by filling a spare target of similar construction with lead, so that the walls bulged in a manner similar to those of the experimental target, and measuring the thickness of this target both by the optical method and by a more convenient micrometer method. The two methods were found to agree to within 0.5%.

The temperature, and hence the density, of the liquid hydrogen was measured in the target cell using carbon-resistance thermometers. This measurement was not made when an electron beam was passing through the target but extensive observations of the rate of scattered electrons as a function of the intensity of the electron beam showed that the presence of the beam had substantially no effect on the target density.

(d) The Scattering Angle

A survey of the scattering angle was carried out using a transit mounted at the center of rotation of the spectrometer and the scattering angle was marked off at intervals of five degrees to an accuracy of 0.01° on brass plates which were fixed to the floor. It was determined that the spectrometer pointed toward its center of rotation to within 0.03° and that the target was centered on the center of rotation well enough so that the consequent uncertainty in the scattering angle was never more than 0.08°. Finally, with the aid of fluorescent screens, it was found that the possible angular variation of the beam direction itself was less than 0.02°.

(e) The Beam Monitor

The electron beam was collected in a Faraday cup situated 9.14 m behind the target. This large distance

[13] The air-bearing pulley was adapted from a design due to H. Bichsel (private communication).

[14] B. Chambers, R. Hofstadter, A. Marcum, and M. R. Yearian, Rev. Sci. Instr. 30, 1019 (1963).

was required so that the cup could be adequately shielded. An evacuated snout extended from the cup to within 51 cm of the target. The charge collected by the cup was accumulated on a bank of calibrated condensers and measured using a vibrating reed electrometer and digital voltmeter. The condensers were known to 0.15% and the digital voltmeter was accurate to 0.1%. The cup itself was slightly modified in order to reduce the loss of charge due to the backward scattering of electrons. For this purpose the inside of the cup was lined with graphite and an improved set of magnets was installed inside the cup in order to prevent the escape of low-energy electrons.

The efficiency of the Faraday cup was measured by comparing its efficiency to that of a smaller, but highly efficient cup, situated temporarily immediately behind the target. For an incident electron energy of 800 MeV, the efficiency of the larger cup relative to the smaller was found to be (99.7±0.3)% and for 350 MeV the relative efficiency was found to be (99.3±0.3)%. A slight reduction in the efficiency of the larger cup as the electron energy decreases is expected due to multiple scattering in the target.

(f) Solid Angle

The solid angle was defined by a pair of 5.08-cm thick lead slits situated approximately 50.8 cm from the target. The distances between these slits and the target were known to 0.15% and the apertures defined by the slits to about 0.4%. Allowing for the diameter of the beam spot, and the uncertainty in its point of intersection with the target, the over-all uncertainty in the solid angle was estimated to be about 0.6%. Careful tests were performed to ensure that all the electrons accepted by the slits were transmitted through the spectrometer and into the counter. The over-all transmission function of the spectrometer was estimated to be 100.0±0.5% for all slit settings used.

(g) Counting Rate Corrections

Since the accelerator provided 60 beam pulses per second, each of approximately 1-μsec duration, and the scaler used in the experiment was unable to count more than one scattered electron per pulse, a correction to the observed counting rate was necessary in order to compensate for dead time losses in the scaler. By restricting the observed counting rate to less than six counts per second, this correction was never allowed to exceed 6.0%. The variation in beam intensity from pulse to pulse was considered in making the correction; and from a study of the observed counting rate as a function of beam intensity, the over-all uncertainty in the final counting rate was estimated to be about 0.05%.

(h) Radiative Corrections

The radiative corrections involved in the elastic-electron scattering process have been calculated by Tsai[15] and for a typical experimental cutoff of 5.5% were of the order of 15%. The contribution to the radiative correction due to electron bremsstrahlung in the target is well known,[16,17] and for the thin target used in the present experiment amounted to only about 3.0%. These corrections are regarded as sufficiently well known so that systematic errors induced by them have been ignored. The ladder counter situated in front of the Čerenkov counter was used to determine the minimum electron momentum accepted by the Čerenkov counter and, therefore, the size of the radiative correction. The error in the determination of this cutoff momentum was considered in the analysis.

TABLE I. An indication of the amount of data accumulated in the measurement of a single cross section. Typically the statistical error on the cross-section measurement was about 2.0%.

Target	Momentum setting	Integrated charge (μC)	Observed counts	Counts normalized to 1800 μC
Hydrogen	Elastic peak	1800.0	4000±63	4000±63
Hydrogen	Radiative tail	800.0	250±16	562±36
Empty	Elastic peak	600.0	80±9	240±27
Empty	Radiative tail	600.0	70±8	210±24
			Corrected counts	4112±82

(i) Counting Statistics

In general, the experimental procedure consisted of four measurements. The spectrometer was first adjusted so that the momentum range accepted by the Čerenkov counter embraced the high-momentum limit of the elastic peak. Then the momentum accepted by the spectrometer was reduced by exactly one full width of the momentum bite of the counter and a second measurement made in the region of the radiative tail. Finally, these two measurements were repeated using an empty target of the same dimensions and wall thickness in order to measure the number of electrons scattered from the target walls. Table I indicates the amount of data accumulated in the measurement of a typical cross section. In this particular case the background contributed about 10% of the total counts observed and the statistical accuracy of the measurement was about 2.0%. The precision and stability of the momentum setting of the spectrometer were such that substantially no error was incurred in assuming that the two momentum ranges accepted by the counter were exactly adjacent.

(j) Summary of Errors

In Table II we summarize the experimental errors, systematic and statistical, which contributed to the

[15] Y. S. Tsai, Phys. Rev. **122**, 1898 (1961).
[16] J. Schwinger, Phys. Rev. **76**, 790 (1949).
[17] H. A. Bethe and J. Ashkin, *Experimental Nuclear Physics*, edited by E. Segrè (John Wiley & Sons, Inc., New York, 1953), Vol. 1, p. 272.

TABLE II. A summary of the sources of systematic error involved in the measurement of a typical cross section at 474 MeV and 60°. The separate systematic errors are regarded as independent and the total systematic error is obtained by taking the square root of the sum of the squares of the separate errors. The total systematic and statistical errors are combined in the same way.

Measured quantity	% systematic error (unless otherwise noted)	% error in cross section
Counter efficiency	0.5	0.5
Beam energy	0.2	0.8
Properties of the target		
Thickness	0.4	
Density	0.3	
Total	0.5	0.5
Scattering angle		
Rotation of spectrometer	0.03°	
Position of entrance slits	0.03°	
Position of beam on target	0.02°	
Total	0.06°	0.8
Beam intensity		
Faraday-cup efficiency	0.3	
Condensers	0.2	
Voltage	0.1	
Total	0.4	0.4
Solid angle		
Distances of slits from target	0.4	
Slit aperture	0.4	
Transmission of spectrometer	0.5	
Total	0.8	0.8
Counting rate correction	0.05	0.05
Radiative correction		
Experimental cutoff	0.3	0.3
	Total systematic error	1.6
	Statistical error	2.0
	Total error	2.6%

measurement of a typical cross section at 474 MeV and 60°.

III. RESULTS

The aim of the present experiment was to measure the elastic electron-proton cross section as a function of scattering angle for various values of q^2 in the range 4.0 to 30.0 F^{-2}. In practice, these measurements were obtained by keeping the scattering angle constant and observing the cross section as a function of the incident-beam energy and, therefore, of q^2. The experimental cross sections and their associated errors are listed in Table III, and shown as a function of energy and angle in Fig. 3. When a particular cross section has been measured more than once only the average result is given.

The elastic electron-proton cross section is given in terms of the incident electron energy E_0 and the scattering angle θ by the Rosenbluth equation,

$$\frac{d\sigma}{d\Omega}=\sigma_{NS}\left\{\frac{(F_{ch}{}^p)^2+(q^2/4M^2)(1+\kappa_p)^2(F_{mag}{}^p)^2}{1+q^2/4M^2}+\frac{2q^2}{4M^2}(1+\kappa_p)^2F_{mag}{}^p\tan^2(\theta/2)\right\}, \quad (2)$$

where

$$\sigma_{NS}=\frac{e^4}{4E_0{}^2}\frac{\cos^2(\theta/2)}{\sin^4(\theta/2)}\frac{1}{[1+(2E_0/M)\sin^2(\theta/2)]},$$

and $F_{ch}{}^p$ and $F_{mag}{}^p$ are respectively the charge and magnetic form factors of the proton normalized to unity at $q^2=0$.[18] κ_p is the anomalous magnetic moment of the proton.

According to Eq. (2), the quantity G_p, defined as the ratio of the observed cross section to the cross section expected from a point proton σ_{NS}, should be a linear function of $\tan^2(\theta/2)$ for a given value of q^2. The observed values of this ratio and its associated errors are given in Table III. In Fig. 4 we show a typical plot of G_p versus $\tan^2(\theta/2)$ for $q^2=7.5$ F^{-2}. At all values of q^2 up to 22.0 F^{-2}, including those shown in Fig. 4, the experimental points can be satisfactorily fitted with a straight line, which is consistent with the assumption of one photon exchange between the electron and proton. The

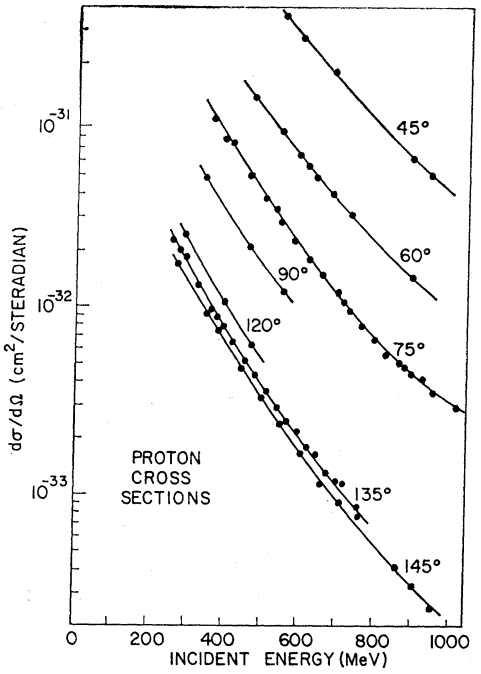

FIG. 3. The absolute electron-proton cross sections measured in the present experiment shown as a function of the incident electron energy and the electron scattering angle. The solid lines shown in this figure represent the predictions of the three-pole fit discussed in Sec. IV.

[18] The quantities $F_{ch}{}^p$ and $F_{mag}{}^p$ are frequently also called G_{Ep} and $G_{Mp}/(1+\kappa_p)$, respectively.

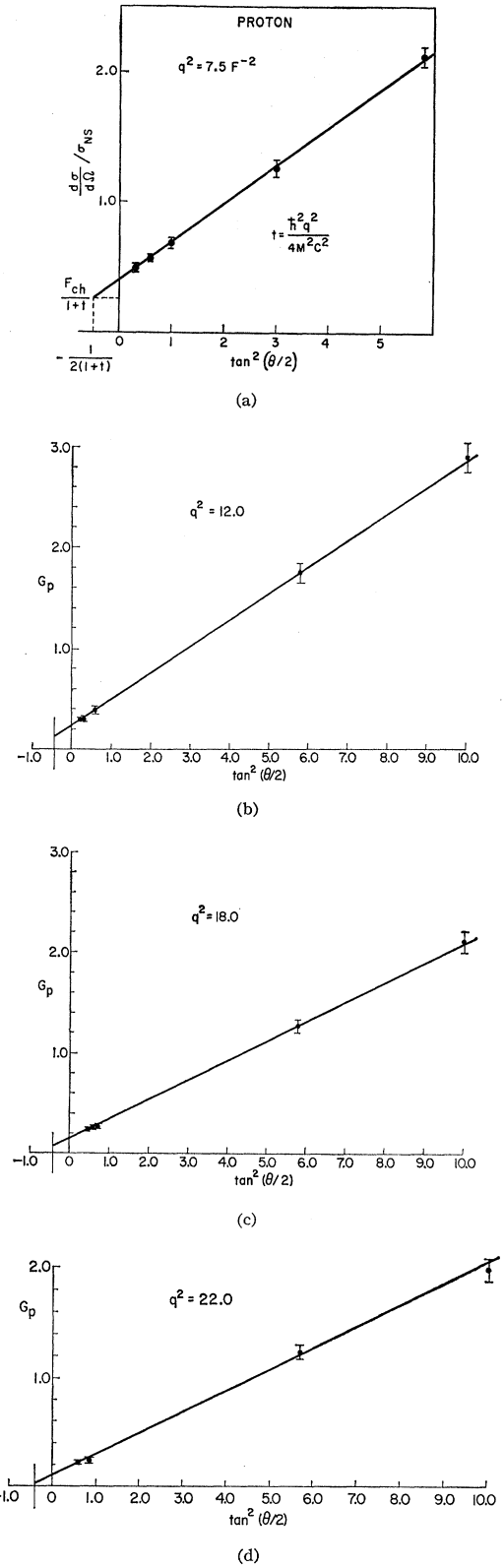

FIG. 4. Examples of Rosenbluth plots for the proton, showing G_p versus $\tan^2(\theta/2)$ for values of q^2 equal to 7.5, 12.0, 18.0, and 22.0 F^{-2}.

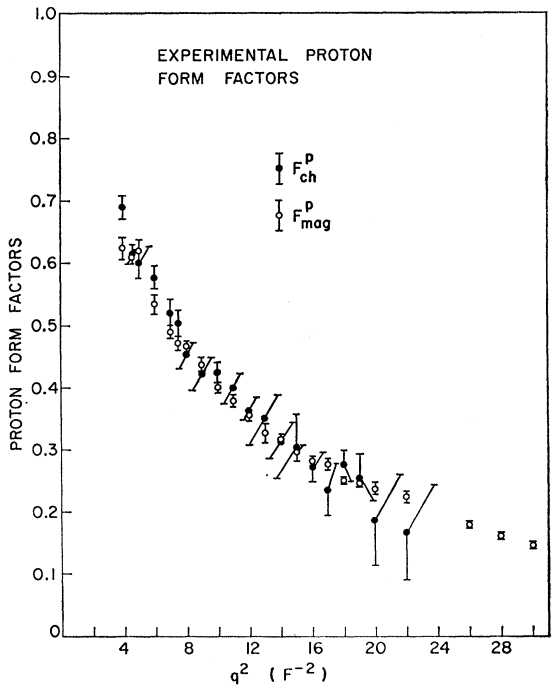

FIG. 5. The experimental values found for the charge and magnetic form factors of the proton as a function of q^2.

validity of the Rosenbluth equation for values of q^2 greater than 22.0 F^{-2} cannot be tested in the present experiment since the data at such large values of q^2 are restricted to the single scattering angle of 145°.

The magnetic form factor of the proton is given by the slope of the straight lines fitted to the data as shown in Fig. 4(a)–(d), and the square of the electric form factor by the ordinate at a small negative value of $\tan^2(\theta/2)$. The values we find for the charge and magnetic form factors are given in Table IV and shown as a function of q^2 in Fig. 5. To within the experimental errors the charge and magnetic form factors, when normalized to unity at $q^2=0$, appear to have the same dependence on q^2 for values of q^2 up to 22.0 F^{-2}. For higher values of q^2, only the magnetic form factor can be determined from the present experimental measurements at 145°. Under these conditions the observed cross section is dominated by the second term in Eq. (2) and the contribution from the first term can be safely neglected.

IV. COMPARISON WITH THEORY

In this section we discuss the degree to which the data of the present experiment can be represented by means of a three-pole approximation to the dispersion theory of nucleon form factors. Kirson[19] and de Vries *et al.*[20] have had considerable success in fitting earlier

[19] M. W. Kirson, Phys. Rev. **132**, 1249 (1963).
[20] C. de Vries, R. Hofstadter, A. Johansson, and R. Herman, Phys. Rev. **134**, B848 (1964).

TABLE III. The absolute experimental cross sections as a function of the incident electron energy and electron scattering angle. The table also indicates the number of times a particular cross section was measured, the experimental cutoff used in determining the radiative correction and the radiative correction factor itself. The final two columns show the value of G_p predicted by the three-pole fit discussed in Sec. IV and the contributions of the individual cross sections to the total value of χ^2.

No. of times measured	q^2 (F^{-2})	Energy (MeV)	Angle (degrees)	Radiative cutoff %	Radiative correction	Cross section (10^{-32} cm^2/sr)	G_p experimental	G_p three-pole fit	χ^2
1	4.0	559.0	45.0	6.0	1.135	35.72	0.635±0.025	0.601	1.7
1	4.0	368.0	75.0	5.8	1.138	9.95	0.733±0.029	0.721	0.2
1	4.0	259.0	135.0	2.4	1.216	2.27	2.150±0.084	2.221	0.7
1	4.6	603.0	45.0	6.0	1.135	26.95	0.564±0.023	0.561	0.0
2	4.6	474.0	60.0	4.0	1.169	13.02	0.558±0.024	0.609	0.8
1	4.6	399.0	75.0	3.7	1.177	7.70	0.677±0.027	0.684	0.1
1	4.6	351.0	90.0	3.5	1.185	4.85	0.790±0.039	0.806	0.2
1	4.6	297.0	120.0	3.8	1.175	2.42	1.362±0.068	1.396	0.2
2	4.6	282.0	135.0	5.7	1.142	1.98	2.280±0.091	2.230	0.3
1	4.6	275.0	145.0	6.1	1.137	1.695	3.460±0.138	3.477	0.0
1	5.0	690.0	40.59	4.8	1.160	29.572	0.526±0.026	0.526	0.0
1	5.0	418.0	75.0	5.9	1.138	7.361	0.720±0.036	0.661	2.7
2	5.0	296.0	135.0	2.3	1.227	1.844	2.390±0.119	2.226	1.9
1	6.0	690.0	45.52	5.6	1.151	17.714	0.523±0.026	0.483	2.4
2	6.0	550.0	60.0	5.9	1.142	8.602	0.540±0.022	0.530	0.2
1	6.0	464.0	75.0	2.4	1.240	4.932	0.611±0.031	0.607	0.0
4	6.0	331.0	135.0	2.4	1.225	1.290	2.175±0.087	2.191	0.0
2	7.0	600.0	60.0	5.6	1.154	6.422	0.490±0.020	0.482	0.2
1	7.0	508.0	75.0	4.2	1.175	3.752	0.570±0.023	0.559	0.2
1	7.0	434.0	95.0	6.9	1.148	1.928	0.682±0.034	0.740	2.9
2	7.0	364.0	135.0	2.5	1.224	0.972	2.060±0.082	2.134	0.8
1	7.0	356.0	145.0	6.0	1.142	0.911	3.440±0.172	3.405	0.0
1	7.5	624.0	60.0	4.8	1.160	5.580	0.465±0.019	0.460	0.1
1	7.5	528.0	75.0	4.2	1.175	3.241	0.540±0.022	0.537	0.0
1	7.5	468.0	90.0	4.1	1.177	2.065	0.653±0.033	0.659	0.0
1	7.5	399.0	120.0	4.8	1.164	1.058	1.200±0.060	1.256	0.9
2	7.5	380.0	135.0	2.5	1.227	0.885	2.080±0.083	2.099	0.1
1	8.0	690.0	55.3	5.7	1.150	5.637	0.403±0.020	0.423	1.0
1	8.0	647.0	60.0	4.3	1.174	4.682	0.424±0.021	0.440	0.6
2	8.0	549.0	75.0	5.8	1.146	2.805	0.510±0.020	0.515	0.1
3	8.0	396.0	135.0	1.8	1.240	0.779	2.020±0.081	2.062	0.3
1	8.0	387.0	145.0	6.1	1.143	0.745	3.450±0.172	3.310	0.7
1	9.0	692.0	60.0	3.9	1.175	3.712	0.392±0.020	0.403	0.3
1	9.0	588.0	75.0	5.7	1.148	2.224	0.475±0.019	0.476	0.0
1	9.0	427.0	135.0	2.5	1.231	0.649	2.022±0.081	1.983	0.2
1	10.0	900.0	46.56	5.7	1.159	5.943	0.349±0.017	0.329	1.4
1	10.0	736.0	60.0	3.8	1.190	3.082	0.374±0.015	0.370	0.1
2	10.0	627.0	75.0	5.7	1.150	1.780	0.440±0.018	0.441	0.0
1	10.0	557.0	90.0	4.3	1.172	1.189	0.567±0.028	0.556	0.2
1	10.0	479.0	120.0	4.4	1.175	0.627	1.100±0.055	1.113	0.1
4	10.0	457.0	135.0	2.3	1.242	0.515	1.890±0.076	1.901	0.0
1	10.0	447.0	145.0	2.4	1.327	0.473	3.110±0.155	3.079	0.0
1	11.0	950.0	46.55	5.7	1.160	4.833	0.320±0.016	0.301	1.5
1	11.0	664.0	75.0	4.3	1.177	1.451	0.410±0.020	0.409	0.0
2	11.0	486.0	135.0	2.4	1.239	0.435	1.860±0.074	1.818	0.3
1	12.0	950.0	49.51	5.6	1.154	3.341	0.294±0.015	0.283	0.5
1	12.0	900.0	53.04	5.7	1.160	2.778	0.298±0.015	0.293	0.1
2	12.0	700.0	75.0	5.6	1.154	1.178	0.377±0.015	0.381	0.1
1	12.0	515.0	135.0	2.0	1.255	0.355	1.750±0.087	1.736	0.0
1	12.0	504.0	145.0	2.4	1.242	0.327	2.900±0.145	2.831	0.2
1	12.5	717.0	75.0	4.1	1.184	1.044	0.354±0.014	0.367	0.9
1	13.0	950.0	52.52	5.6	1.154	2.442	0.283±0.014	0.269	1.0
1	13.0	735.0	75.0	4.1	1.186	0.941	0.338±0.014	0.355	1.5
1	13.0	543.0	135.0	2.4	1.242	0.290	1.635±0.082	1.657	0.1
1	14.0	950.0	55.6	5.8	1.133	1.833	0.278±0.014	0.257	2.3
1	14.0	900.0	59.8	5.8	1.163	1.429	0.271±0.014	0.269	0.0
2	14.0	769.0	75.0	5.4	1.159	0.787	0.315±0.013	0.331	1.6
1	14.0	570.0	135.0	2.3	1.248	0.247	1.575±0.079	1.581	0.0
1	14.0	559.0	145.0	2.4	1.245	0.237	2.730±0.136	2.590	1.1
1	15.0	950.0	58.75	5.4	1.158	1.337	0.264±0.013	0.247	1.6
1	15.0	802.0	75.0	3.7	1.196	0.664	0.294±0.015	0.309	1.1
1	15.0	597.0	135.0	2.4	1.245	0.214	1.535±0.077	1.507	0.1
1	16.0	950.0	62.0	5.6	1.157	0.928	0.238±0.012	0.240	0.0
1	16.0	900.0	67.0	5.6	1.160	0.771	0.255±0.013	0.257	0.0
1	16.0	835.0	75.0	4.2	1.185	0.554	0.270±0.013	0.290	2.2
1	16.0	802.0	80.0	2.4	1.242	0.516	0.318±0.016	0.315	0.0
1	16.0	624.0	135.0	2.6	1.240	0.178	1.425±0.071	1.438	0.0
1	16.0	612.0	145.0	2.5	1.243	0.164	2.380±0.119	2.365	0.1

TABLE III (*continued*)

No. of times measured	q^2 (F^{-2})	Energy (MeV)	Angle (degrees)	Radiative cutoff %	Radiative correction	Cross section (10^{-32} cm^2/sr)	G_p experimental	G_p three-pole fit	χ^2
1	17.0	950.0	65.36	5.5	1.158	0.716	0.238±0.012	0.235	0.1
1	17.0	867.0	75.0	4.6	1.177	0.498	0.266±0.013	0.272	0.2
1	17.0	651.0	135.0	2.0	1.267	0.163	1.455±0.073	1.372	1.3
1	17.5	883.0	75.0	4.0	1.190	0.479	0.267±0.011	0.264	0.1
1	18.0	950.0	68.89	5.5	1.160	0.565	0.244±0.012	0.232	1.0
1	18.0	899.0	75.0	3.0	1.193	0.444	0.259±0.013	0.256	0.1
1	18.0	864.0	80.0	2.3	1.251	0.364	0.269±0.013	0.279	0.5
1	18.0	677.0	135.0	2.1	1.263	0.129	1.275±0.064	1.309	0.3
1	18.0	664.0	145.0	2.4	1.254	0.119	2.120±0.106	2.160	0.1
1	19.0	950.0	72.58	5.6	1.159	0.416	0.234±0.012	0.231	0.1
1	19.0	930.0	75.0	5.0	1.172	0.415	0.263±0.016	0.241	2.0
2	19.0	703.0	135.0	2.4	1.248	0.118	1.280±0.064	1.250	0.2
1	20.0	961.0	75.0	5.6	1.157	0.349	0.239±0.012	0.227	1.0
1	20.0	950.0	76.47	2.4	1.240	0.340	0.250±0.012	0.233	1.9
1	20.0	925.0	80.0	2.2	1.262	0.259	0.226±0.011	0.248	3.8
1	20.0	900.0	83.8	1.8	1.240	0.232	0.242±0.012	0.267	4.2
1	20.0	728.0	135.0	2.5	1.247	0.115	1.370±0.068	1.194	6.6
1	20.0	715.0	145.0	2.4	1.253	0.0903	1.940±0.097	1.974	0.1
1	22.0	1022.0	75.0	4.2	1.189	0.2819	0.224±0.011	0.202	3.8
1	22.0	950.0	85.05	5.4	1.163	0.1825	0.235±0.014	0.245	0.5
1	22.0	779.0	135.0	2.4	1.257	0.0882	1.240±0.062	1.091	5.8
1	22.0	764.0	145.0	2.4	1.255	0.0777	1.990±0.099	1.808	3.4
1	26.0	862.0	145.0	2.4	1.271	0.0432	1.515±0.082	1.524	0.0
1	28.0	910.0	145.0	2.3	1.276	0.0325	1.315±0.092	1.404	0.9
1	30.0	958.0	145.0	2.3	1.265	0.0249	1.150±0.092	1.296	2.5

data on proton and neutron form factors to a model of this type.

For theoretical reasons it is convenient to resolve the nucleon form factors into their isotopic components which are defined in Eq. (3),

$$\begin{aligned} G_{ES}&=\tfrac{1}{2}(F_{\mathrm{ch}}{}^p+F_{\mathrm{ch}}{}^n)\,,\\ G_{EV}&=\tfrac{1}{2}(F_{\mathrm{ch}}{}^p-F_{\mathrm{ch}}{}^n)\,,\\ G_{MS}&=\tfrac{1}{2}[(1+\kappa_p)F_{\mathrm{mag}}{}^p+\kappa_n F_{\mathrm{mag}}{}^n]\,,\\ G_{MV}&=\tfrac{1}{2}[(1+\kappa_p)F_{\mathrm{mag}}{}^p-\kappa_n F_{\mathrm{mag}}{}^n]\,. \end{aligned} \tag{3}$$

If it is assumed that the behavior of the isoscalar nucleon form factors is dominated by intermediate states coupled to the ω and ϕ mesons and that the behavior of the isovector form factors is likewise dominated by the effects of the ρ meson, then the expressions for the isotopic form factors can be written in the following way:

$$\begin{aligned} G_{ES}&=0.5\left\{\frac{s_{e1}}{1+q^2/15.7}+\frac{s_{e2}}{1+q^2/26.7}+(1-s_{e1}-s_{e2})\right\}\,,\\ G_{MS}&=0.44\left\{\frac{s_{m1}}{1+q^2/15.7}+\frac{s_{m2}}{1+q^2/26.7}+(1-s_{m1}-s_{m2})\right\}\,, \end{aligned} \tag{4}$$

and

$$G_{EV}=0.5\left\{\frac{v_{e1}}{1+q^2/M_p{}^2}+(1-v_{e1})\right\}\,,$$

$$G_{MV}=2.353\left\{\frac{v_{m1}}{1+q^2/M_p{}^2}+(1-v_{m1})\right\}\,,$$

where the constant terms represent the contribution from nonresonant intermediate states or states of higher mass and the parameters S_{e1}, S_{e2}, S_{m1}, S_{m2}, V_{e1}, and V_{m1} determine the strengths with which the various terms contribute. The constant terms can be expressed in terms of the parameters S_{e1}, S_{e2}, S_{m1}, S_{m2}, V_{e1}, and V_{m1}

TABLE IV. The experimental determinations of the proton form factors as a function of q^2. For comparison we also give the form factors predicted by the three-pole fit to the results of the present experiment.

q^2 (F^{-2})	Experimental values $F_{\mathrm{ch}}{}^p$	Experimental values $F_{\mathrm{mag}}{}^p$	Three-pole fit $F_{\mathrm{ch}}{}^p$	Three-pole fit $F_{\mathrm{mag}}{}^p$
4.0	0.689±0.019	0.623±0.018	0.658	0.644
4.6	0.615±0.015	0.611±0.010	0.624	0.610
5.0	0.599±0.026	0.618±0.021	0.603	0.588
6.0	0.577±0.019	0.533±0.014	0.554	0.540
7.0	0.521±0.021	0.490±0.010	0.511	0.499
7.5	0.504±0.022	0.472±0.011	0.492	0.480
8.0	0.453±0.020	0.466±0.009	0.474	0.462
9.0	0.422±0.027	0.437±0.011	0.440	0.430
10.0	0.424±0.017	0.400±0.007	0.410	0.402
11.0	0.398±0.025	0.379±0.009	0.383	0.376
12.0	0.363±0.020	0.355±0.007	0.359	0.354
13.0	0.349±0.040	0.327±0.015	0.337	0.333
14.0	0.315±0.028	0.316±0.008	0.317	0.314
15.0	0.304±0.053	0.297±0.015	0.299	0.297
16.0	0.271±0.024	0.282±0.006	0.283	0.282
17.0	0.234±0.041	0.277±0.008	0.267	0.268
18.0	0.274±0.026	0.250±0.005	0.253	0.254
19.0	0.254±0.039	0.245±0.008	0.240	0.242
20.0	0.187±0.073	0.237±0.010	0.228	0.231
22.0	0.166±0.075	0.224±0.007	0.207	0.211
26.0		0.178±0.005	0.171	0.179
28.0		0.160±0.006	0.157	0.166
30.0		0.145±0.006	0.144	0.154

by the requirements that the isotopic form factors reduce to their known static values.

We have investigated the degree to which a three-pole approximation to the nucleon form factors of the type given by Eq. (4) can be made to fit the data of the present experiment. The ω and ϕ mesons are assigned their well-defined observed masses but the mass of the ρ meson is treated as an adjustable parameter in view

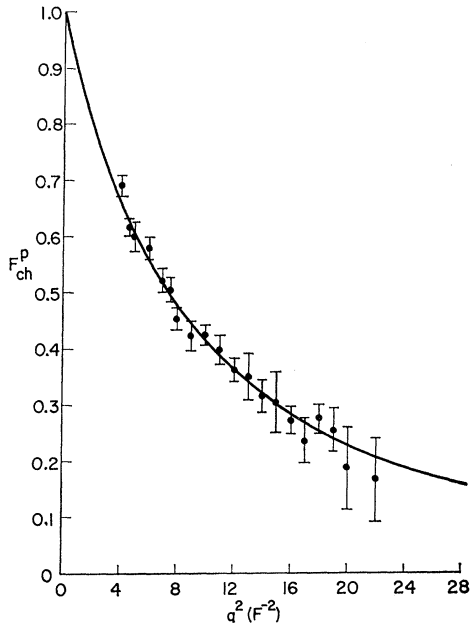

FIG. 6. (a) A comparison between the proton charge form factors measured in the present experiment and those predicted by the three-pole fit to the experimental cross section discussed in Sec. IV. (b) A comparison between the proton magnetic form factors measured in the present experiment and those predicted by the three-pole fit to the experimental cross section discussed in Sec. IV.

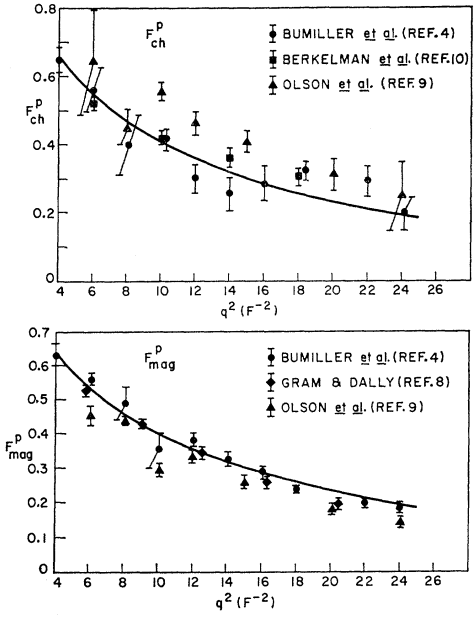

FIG. 7. A comparison between the results of the present experiment and the results of previous experiments in the same q^2 range.

of the large observed width of this resonance. The total number of free parameters is reduced to six by imposing the condition

$$\left(\frac{dF_{ch}{}^n}{dq^2}\right)_{q^2=0}=0.021\ \mathrm{F}^{-2}, \tag{5}$$

as required by the neutron-electron interaction.[21]

The fitting procedure compares electron-proton cross sections measured in the present experiment with those computed from a trial set of parameters through Eqs. (3) and (4). The statistical function χ^2 is computed and then minimized as a function of the six free parameters using an IBM 7090 computer. The following best fit is obtained which corresponds to a value of χ^2 of 78 for 87 degrees of freedom.

$$\begin{aligned}
G_{ES}&=0.5\left\{\frac{2.50}{1+q^2/15.7}-\frac{1.60}{1+q^2/26.7}+0.10\right\},\\
G_{MS}&=0.44\left\{\frac{3.33}{1+q^2/15.7}-\frac{2.77}{1+q^2/26.7}+0.44\right\},\\
G_{EV}&=0.5\left\{\frac{1.16}{1+q^2/8.19}-0.16\right\},\\
G_{MV}&=2.353\left\{\frac{1.11}{1+q^2/8.19}-0.11\right\}.
\end{aligned} \tag{6}$$

[21] D. J. Hughes, L. A. Harvey, M. D. Goldberg, and M. J. Stafner, Phys. Rev. **90**, 497 (1953).

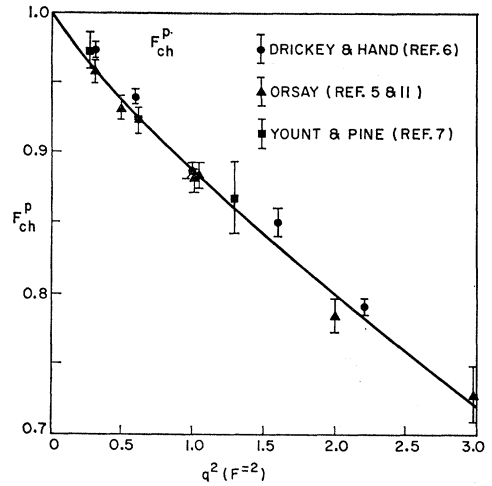

FIG. 8. A comparison between the experimental determinations of the proton form factors in the q^2 range less than 4.0 F^{-2} and the predictions of the three-pole fit to the results of the present experiment.

The values of the ratio G_p predicted by Eqs. (6) are listed in Table III for comparison with the experimental values together with the contribution of each measured cross section to the total value of χ^2. A comparison between the measured form factors and those predicted by Eqs. (6) is shown in Fig. 6(a) and (b). A satisfactory representation of the behavior of the proton form factors for values of q^2 up to 30.0 F^{-2} can therefore be given by such a three-pole model. For the purposes of the present paper we regard Eqs. (6) as providing a convenient and accurate representation of the proton form factors and of the elastic electron-proton cross sections in the q^2 range from 4.0 to 30.0 F^{-2} and for electron scattering angles in the range from 45 to 145°. A discussion of the physical significance of Eqs. (6) is given in a recent paper in which we give the results of a similar fit to the results of both the present experiment and an experiment of comparable precision designed to measure the electromagnetic form factors of the neutron.[22]

[22] E. B. Hughes, T. A. Griffy, M. R. Yearian, and R. Hofstadter, Phys. Rev. **139**, B458 (1965).

A comparison between the results of the present experiment and the results of previous experiments in the same q^2 range is shown in Fig. 7. The agreement is generally good with the exception of the early data of Olson *et al.*,[9] which appear to differ systematically from the results of the present experiment. In Fig. 8 we show a similar comparison between earlier measurements of the proton form factors for values of q^2 less than 4.0 F^{-2} and the form factors predicted by an extrapolation of Eqs. (6) into the low-q^2 range. The agreement is excellent.

V. CONCLUSIONS

In the present experiment, absolute measurements of the elastic electron-proton cross section have been made with an accuracy of about 4% in the q^2 range from 4.0 to 30.0 F^{-2}. These measurements have been used to verify the Rosenbluth equation for values of q^2 up to 22.0 F^{-2} and to determine the form factors of the proton with a precision exceeding that obtained in previous experiments. There is good agreement between the results of the present experiment and those of the earlier experiments. It is found that the charge and magnetic form factors of the proton have the same dependence on q^2 within the accuracy with which they are determined. It is also shown that an acceptable representation of the behavior of the proton form factors in the above q^2 range can be given in terms of a three-pole approximation to the dispersion theory of nucleon form factors, and that the extrapolation of this representation into the region of q^2 less than 4 F^{-2} is in excellent agreement with the experimental results.

ACKNOWLEDGMENTS

The authors would like to thank the members of the staff of the High Energy Physics Laboratory and the graduate students of Professor Hofstadter's group at Stanford University for their invaluable help throughout the course of this experiment. They are particularly indebted to R. Ryneveld and R. Parks for their assistance with the experimental equipment.